Article

Not peer-reviewed version

Transplanted Murine Tumours SPECT Imaging with ^{99m}Tc Delivered with an Artificial Recombinant Protein

Natalia V. Pozdniakova *, Alexey A. Lipengolts, Vsevolod A. Skribitsky, Kristina E. Shpakova, Yulia A. Finogenova, Anna V. Smirnova, Alexei B. Shevelev, Elena Y. Grigorieva

Posted Date: 9 August 2024

doi: 10.20944/preprints202408.0697.v1

Keywords: SPECT; de novo protein design; technetium; targeted delivery; cancer; in vivo imaging

Article

Transplanted Murine Tumours SPECT Imaging with ^{99m}Tc Delivered with an Artificial Recombinant Protein

Natalia V. Pozdniakova [1,2,*], Alexey A. Lipengolts [1,3], Vsevolod A. Skribitsky [1,3], Kristina E. Shpakova [1,3], Yulia A. Finogenova [1], Anna V. Smirnova [1], Alexei B. Shevelev [2] and Elena Y. Grigorieva [1]

[1] N.N. Blokhin National Medical Research Center of Oncology of the Ministry of Public Health of the Russian Federation (N.N. Blokhin NMRCO), Kashirskoe Shosse, 23, 115478 Moscow, Russia; natpo2002@mail.ru (N.V.P.)

[2] N.I. Vavilov Institute of General Genetics RAS, Gubkina Street, 3, GSP-1, 119991 Moscow, Russia; shevel_a@hotmail.com (A.B.Sh.)

[3] National Research Nuclear University MEPhI, Institute of Engineering Physics for Biomedicine (PhysBio), Kashirskoe Shosse, 31, 115409 Moscow, Russia

* Correspondence: natpo2002@mail.ru; Tel.: +7-977-767-99-90

Abstract: ^{99m}Tc is a well-known radionuclide widely used and readily available for medical imaging. Despite this, the ^{99m}Tc isotope is rarely utilized for tumour imaging due to the lack of agents that can selectively deliver it to tumours. However, the use of immunologically compatible recombinant proteins, which combine metal-binding sites and tumour-specific ligands, shows promise for utilizing ^{99m}Tc in the early detection of tumours. To illustrate this, a protein called E1b, containing a metal binding center with ELP repeats, tumour-specific ligands recognizing integrin $\alpha v\beta 3$ and nucleolin, as well as a short Cys-rich sequence, was artificially designed. This protein was produced in *E. coli* and purified to homogeneity using metal-chelate chromatography. In experiments, C57Bl/6 and Balb/C mice with subcutaneously grafted lung carcinoma (LLC) or mammary gland adenocarcinoma (Ca755, EMT6, or 4T1) were used to test ^{99m}Tc-E1b selectivity and the kinetics of isotope retention. The mice were intravenously injected with approximately 80 MBq of ^{99m}Tc in complex with E1b, which had been freshly purified using gel-chromatography. The biodistribution of the labeled protein was then studied using the SPECT/CT imaging method within 24 h. The ratio of radionuclide distribution in the tumour versus the adjacent normal tissue (T/N) steadily increased over the 24-h period, reaching 15.7±4.2 for EMT6, 16.5±3.8 for Ca755, 6.7±4.2 for LLC, and 7.5±3.1 for 4T1.

Keywords: SPECT; de novo protein design; technetium; targeted delivery; cancer; in vivo imaging

1. Introduction

^{99m}Tc isotope offers a balance between patient safety and efficient visualization of tumours using single-photon emission computed tomography (SPECT/CT). Most commercial radiochemical preparations for delivering ^{99m}Tc to tumours use methylene diphosphonate (MDP) [1,2] and zoledronic acid [3]. These preparations work for all types of tumours and are cost-effective for a wide range of patients. However, they are cleared from the body quickly and may not be completely safe, prompting a need for more specific delivery methods for the isotope to tumour sites.

1.1. Tumour Targeting

A history of delivering ^{99m}Tc to tumours begins with attaching it to tumour-specific monoclonal antibodies, which are modified with bifunctional SH-containing cross-linkers [4]. After reduction, the

 doi:10.20944/preprints202408.0697.v1

isotope binds to the protein by forming bonds with sulfhydryl groups. Since random chemical modification of antibodies by linker or chelator molecules can lead to a decrease in their specificity, the authors overcame this limitation by attaching the chelator at glycosylation sites located at well-defined sites on humanized antibodies.

In a recent paper by Li et al. [5], an alternative approach was performed for site-directed modification of the antibodies. The authors developed ^{99m}Tc-labeled humanized antibodies targeting the cancer marker HER-2 (epidermal growth factor receptor). They used G4EC-type peptides as chelator molecules, which they bound to the antibody by enzymatic transacylation with Sortase A precisely at the site of an artificially introduced LPETG motif. They reported distribution of the isotope in mice with grafted tumours by using SPECT imaging and ex vivo radiometry. The tumour uptake of ^{99m}Tc for various antibodies ranged from 8.03±0.95 to 14.69±1.31 %ID/g. Meanwhile, for two different antibody preparations, the maximum accumulation in the tumour occurred 1 h after drug administration, and for another antibody, it was found 4 h after administration. The kidney uptake of the fast-binding MIRC208 antibody was 352.68±30.31 and 281.47±31.80 %ID/g 1 and 2 h after the drug administration, respectively. The accumulation of the antibodies in the liver was slower than in the kidneys, but the retention time in the liver was longer than in other organs. It's worth noting that the injected radionuclide dose used in the work [5] was 5.6 MBq/kg of body weight.

Enzymatic modification of antibodies was also described in [6]. To improve the pharmacokinetic characteristics of drugs designed for imaging tumour-associated macrophages, the authors hydrolyzed antibodies using highly specific peptidases (Papain or IdeS), and then bound a chelator to the fragments of interest to provide isotope binding. The ^{99m}Tc labeled preparations obtained in this way varied significantly in their clearance time (in range from 1 to 22 h).

Some of them provided efficient visualization of the tumours in the mice as early as 1 h after administration [5,6].

Beyond massive protein molecules such as antibodies and their fragments, tumour-specific peptides, both naturally occurring and those obtained by peptide synthesis, are also used for targeting.

In a study by Delvaeye et al. [7], SPECT imaging with ^{99m}Tc-labeled duramycin was used to visualize inflammation caused by the systemic administration of TNFα to mice. Duramycin is a 19 a.a. tetracyclic antimicrobial peptide containing non-proteinaceous amino acids and belonging to a family of lantibiotics. It is produced by *Streptomyces cinnamoneus*. The duramycin can bind to membranes containing phosphatidylethanolamine, a specific lipid marker of tumour vasculature commonly used for targeting tumour lesions [8]. SPECT/CT scans were conducted 4, 6, and 8 h after injecting ^{99m}Tc-labeled duramycin, and the standardized uptake value (SUV) was calculated to assess biodistribution in vivo. The biodistribution was analyzed by ex vivo radiometry. Notably, in this study, the SUV index for the lungs, liver, kidneys, and intestines remained relatively constant over the whole survey period, with values of 0.55 for the lungs, 1.0-1.2 for the liver, 0.75 for the small intestine, and approximately 3.0 for the kidneys. In control animals that had not received TNFα injections, the isotope excretion from all studied organs, except the kidneys, occurred significantly faster. Clinical trials have been conducted on ^{99m}Tc-duramycin complexes as contrast agents for SPECT/CT, showing favorable safety and slow clearance due to their tight binding with plasma proteins. However, ^{99m}Tc-duramycin complexes are primarily recommended for assessing the efficacy of tumour therapy rather than for visualizing primary tumour foci [9]. This limitation exists because the duramycin may target sources other than tumour e.g. vasculature, leading to false-positive results in tumour screening by SPECT/CT, which may be caused by non-tumour necrosis or infection foci in patients.

An instance of using a similar technology is reported by Chapeau et al. [10], where three different synthetic tumour-specific peptides conjugated with cyclic ligands were used to deliver ^{203}Pb and ^{212}Pb to NCI-H69 tumour-bearing mice. All compounds showed nanomolar affinity (2.5–3.1 nM) for somatostatin receptor subtype 2 (SSTR2). SPECT/CT images revealed high tumour uptake at 1, 4, and 24 h post-injection of [^{203}Pb]-eSOMA-01/02. Ex vivo biodistribution studies confirmed that the highest uptake in tumours was observed with [^{212}Pb]-eSOMA-01. [^{212}Pb]-eESOMA-01 provided the highest

 doi:10.20944/preprints202408.0697.v1

absorbed dose in the tumour (35.49 Gy/MBq) along with the lowest absorbed dose in the kidneys (121.73 Gy/MBq) in comparison to other tested radioligands. The authors conclude that [^{212}Pb]-eSOMA-01 is a promising candidate for targeting isotopes acting as alpha radiation sources to the neuroendocrine tumours.

In addition to tumour-specific antibodies and peptides, the use of serum albumin as a targeting molecule is also of interest. The paper [11] discusses SPECT imaging of multifocal mouse hepatocarcinoma using ^{99m}Tc-labeled albumin nanoparticles with a diameter of less than 200 nm. The administered dose was 87.2±8.3 MBq per animal. The ^{99m}Tc SUV values in the livers of different groups of animals ranged from 6.2 to 11.2.

1.2. Approaches to ^{99m}Tc Binding with Address Molecules

As can be seen from the above, labeling of an address molecule with ^{99m}Tc requires the presence of certain chemical groups in its structure. Thus, ^{99m}Tc can bind to the SH-group of proteins and peptides, either of natural origin or introduced artificially as a part of a linker (see above [3]). High affinity chemical chelators, are also used to immobilize ^{99m}Tc [12,13]. This also requires an additional step of chemical modification of the address molecule. There is an example [14] as well reporting the possibility of creating stable ^{99m}Tc complexes with recombinant proteins containing His-tags for purification using immobilized metal affinity chromatography (IMAC). To enhance the binding of ^{99m}Tc to His-tags, the authors [14] proposed using metal ion complexes with compounds containing a triplicated carbonyl group.

Summarizing the abovementioned, the conclusion drawn is that so far there are no commonly available contrast agents for the primary diagnosis of all types of tumours by SPECT/CT. Bi-phosphonate derivatives are not safe and are excreted rapidly. The actively promoted duramycin derivatives render false-positive responses, while derivatives of monoclonal antibodies and oncomarker-specific peptides recognize only certain types of tumours, which is unacceptable at the stage of diagnostics when the tumour type and even the existence of a tumour is unknown.

In our previous study, we discussed the creation of W-family proteins with multiple metal-binding centers and tumour-specific ligands, RGD (Arg-Gly-Asp) and F3-peptide (nucleolin-binding peptide) [15]. The protein elements were derived from the human proteome to ensure compatibility with the human body. The amino acid composition was carefully designed to prevent aggregation and non-specific binding in the bloodstream. RGD/F3-containing proteins have the potential to be used for developing new ^{99m}Tc-based radiopharmaceuticals for diagnosing primary tumours. In this study, a W4 protein, called E1b, was modified by removing GFP and adding a cysteine cluster at the C-terminus to enhance its bonding with ^{99m}Tc [13].

We aimed to assess the effectiveness of using the ^{99m}Tc-labeled E1b protein for tumour detection with SPECT/CT. We also considered the presence of a 7His-tag in the E1b protein, which could further contribute to bonding with ^{99m}Tc [14]. To evaluate E1b's ability to deliver ^{99m}Tc to tumours in vivo, we used four murine tumour models (lung carcinoma LLC, mammary gland adenocarcinomas Ca755, EMT6, and 4T1). We calculated the SUV for the tumour node and adjacent muscle and used the T/N ratio as an indicator of diagnostic efficacy. Additionally, SUV for all key organs (such as the heart, lungs, liver, kidneys, bladder, bowel, stomach, muscle, brain, salivary glands, and thyroid glands) was assessed to elucidate the protein's biodistribution in the mouse body and to identify routes of the isotope excretion. Free sodium pertechnetate was used as a preparation of comparison in this experiment.

It's important to note that unlike most of the cited publications, our study did not involve using mice with severe combined immunodeficiency (SCID) and xenografts of human tumours. While this approach makes it challenging to extrapolate the data to human tumours, which have different markers compared to mice [16], it offers advantages due to the affordability and ease of working with non-immunodeficient mouse lines. This approach enables obtaining significant amounts of data at the early stages of developing new tools for tumour diagnosis and therapy.

The results suggest that further exploration of artificial recombinant proteins could lead to promising diagnostic and therapeutic radiopharmaceuticals for experimental and clinical oncology.

 doi:10.20944/preprints202408.0697.v1

2. Results

2.1. Novel Recombinant Artificial Protein E1b

In this study, we introduce the ^{99m}Tc carrier protein E1b for the first time. It's distinct from the previously described 13W4 protein in that it lacks the GFP fluorescent protein in the C-terminal position. Instead, it features a Cys-rich 12 a.a. flexible peptide (GlyGlyGlyCys)3 (further Cys-rich peptide) in that position. The E1b protein has a theoretically calculated MW=25.7 kDa and contains functional elements specified in Table 1.

Table 1. Stoichiometry of functional elements in E1b ^{99m}Tc carrier protein.

Functional elements	Number per molecule	Function
His-taq	1	Protein purification by IMAC
RGD-motif	3	Binding integrin αVβ3
F3-peptide	1	Nucleolin ligand binding
Metal binding site (Mbs)	4	Radionuclide binding in coordinated complex
Free cysteine	3	Radionuclide covalent coupling
ELP repeats (5 a.a.)	13	Immune-compatible molecular framework

The overall structure of the E1b protein elements, the SDS-PAGE data demonstrating its purity, and the functional map of the pE1b plasmid construct used for producing E1b in *E. coli* are depicted in Figure 1 (please refer to Supplementary files Fugure S1_Electropherogram of the purified E1b protein and pE1b plasmid map).

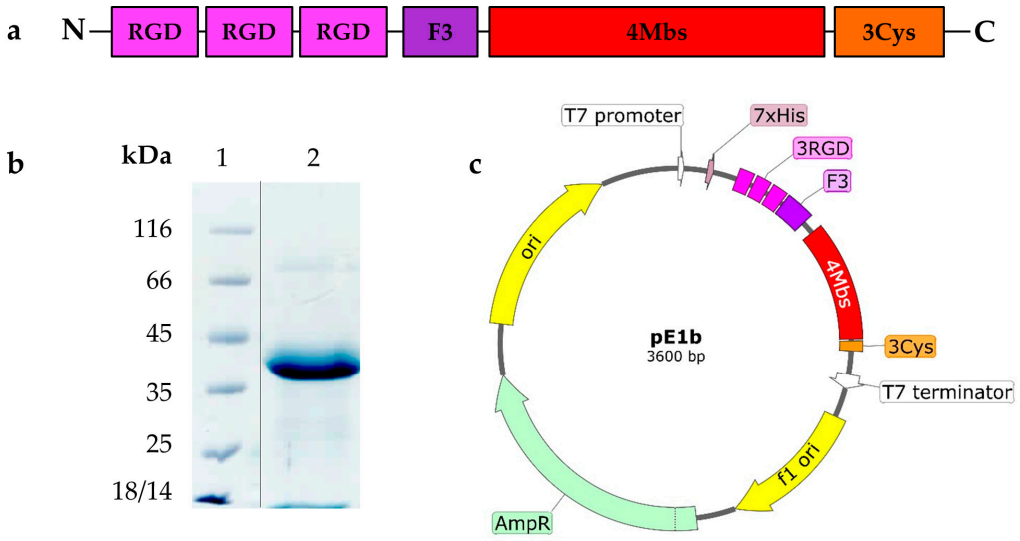

Figure 1. E1b artificial protein, its production and purification. (a) Block-scheme of functional elements composing E1b protein; (b) electropherogram of the purified E1b protein used as ^{99m}Tc carrier in biological trials (electrophoresis was carried out in 12.5% PAAG supplemented with SDS and stained with Coomassie R-250; lanes: 1 - molecular mass standard (Fermentas, Lithuania), 2 - purified E1b (vertical black line indicates spliced lines of the same gel)); (c) plasmid map pE1b, generated with SnapGene Viewer; Element legend - 3×RGD - three tandem RGD-containing peptides, F3 - F3 peptide, 4MBS – four metal-binding sites alternating with ELP-repeats, 3Cys – C-terminal Cys-rich peptide.

 doi:10.20944/preprints202408.0697.v1

The E1b protein yield from the recombinant *E. coli* NiCo21 (DE3, pE1b) strain reached 18-20 mg/L culture, and it was present only in a soluble form. The apparent molecular weight (MW) of the E1b protein, as indicated by SDS-PAGE data (see Figure 1b), was approximately 40 kDa, which is significantly higher than the theoretical expectation of 25.7 kDa. We suspect that this discrepancy is due to the unusually low content of hydrophobic amino acids in comparison to most natural proteins. Following a simple process of immobilized metal ion affinity chromatography (IMAC) and dialysis, we obtained a solution of E1b protein with a concentration of 3.3 mg/ml (equivalent to 127.61 μM). According to Table 1, this solution contains 510.4 μM of potential coordination-type ^{99m}Tc-binding sites and 382.3 μM of potential covalent-linkage sites. The electrophoretic purity of the preparation was determined to be 95%. In addition, the protein was found to contain approximately 390 μM of free sulfhydryl moieties as per the DTNB assay (refer to Materials and Methods). Thanks to the described process, we were able to produce a protein preparation with high activity in a short period (refer to Figure 2).

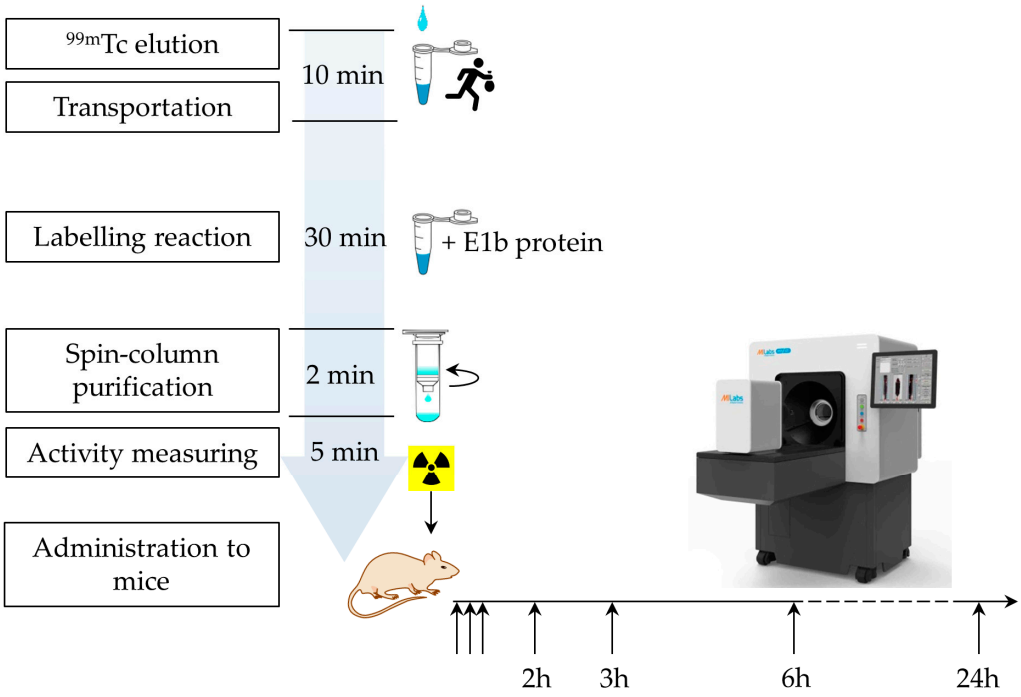

Figure 2. Timing of the protein labeling procedure and the *in vivo* experiment.

2.2. Biodistribution of ^{99m}Tc-E1b Protein in Mice

The biodistribution of ^{99m}Tc-E1b in Balb/C mice was analyzed using the SPECT/CT method in vivo (refer to Appendix A). The labeled protein was injected intravenously into the mice. To measure the compound's presence in the blood, the average radioactivity in the heart chambers was calculated. Following intravenous administration, the compound was swiftly removed from the bloodstream: immediately after injection, the heart's SUV reached 3.5±0.3, then dropped rapidly to 0.6±0.5 after 3 h, and decreased further to a background value of 0.1±0.1 by 24 h. Immediately after the injection, there was a moderate uptake of ^{99m}Tc-E1b in the lungs (SUV up to 1.8±0.1) and in the liver (SUV up to 1.8±0.2). Subsequently, within 24 h, the lung radioactivity returned to the background value, while it remained slightly elevated in the liver (SUV 0.3±0.1). By 6 h post-injection, a notable accumulation of radioactivity was observed in parts of the colon containing feces (SUV up to 1.2±0.1). Based on the data, there is evidence of at least partial hepatobiliary excretion of ^{99m}Tc. High activity in the kidneys was detected from the first minute after administration (SUV 14±1), with the radionuclide uptake primarily along the cortical layer of the kidneys. Activity in the kidneys

 doi:10.20944/preprints202408.0697.v1

increased over time and peaked at 3 h after injection (SUV 24±6) (Figure 3a), followed by a decrease to SUV 13±1 by 24 h. At 3 h post-injection, high activity was also observed in the bladder (Figure 3b), which suggests a predominantly renal route of ^{99m}Tc excretion. There were no indications of ^{99m}Tc-E1b accumulation in muscle tissue or in the brain.

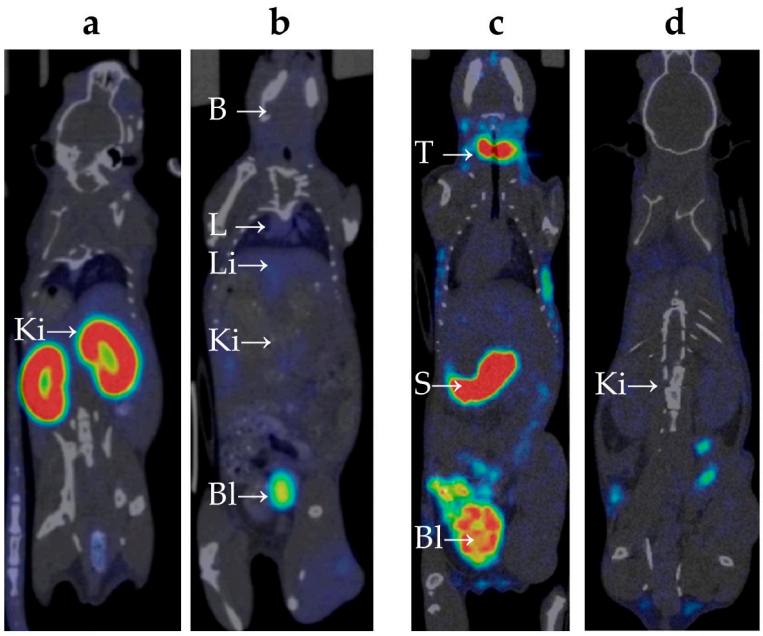

Figure 3. SPECT/CT scan of the mice 3 h after intravenous administration of the radiopharmaceutical compound. The images taken after administration of ^{99m}Tc-E1b show strong accumulation in the kidneys, mainly in the renal cortex (a), low accumulation in the lungs and liver, no accumulation in the stomach, and strong accumulation in the bladder (b). Images taken after ^{99m}Tc-pertechnetate administration show strong accumulation in the thyroid gland, stomach, and bladder, low accumulation in the liver (c), and low accumulation in the kidneys (d). The labels used are: B for brain, L for lung, Li for liver, Bl for urinary bladder, Ki for kidney, T for thyroid gland, and S for stomach.

Although only healthy mice were used for the quantitative biodistribution study, the SPECT data revealed a similar biodistribution pattern in both healthy and tumour-bearing mice.

2.3. Biodistribution of ^{99m}Tc-Pertechnetate in Mice

The behavior of free ^{99m}Tc-pertechnetate and the synthesized ^{99m}Tc-E1b protein in the bodies of Balb/C laboratory mice was evaluated using dynamic SPECT/CT (refer to Supplementary file S2_table_Summary of SUV values). ^{99m}Tc-pertechnetate, a commonly used radiopharmaceutical drug for thyroid and salivary gland scintigraphy, as well as for the preparation of other radiopharmaceuticals, was chosen as a reference. After intravenous injection of ^{99m}Tc-pertechnetate, the maximum activity in the heart chambers, reflecting the content of ^{99m}Tc-pertechnetate in the blood, reached SUV 1.9±0.3. This was followed by a gradual decrease, with the SUV decreasing to 0.7±0.2 after 3 h, and returning to the background level of 0.1±0.1 after 24 h.

Significant accumulation of ^{99m}Tc-pertechnetate in the neck area was observed (refer to Figure 3c), which increased over time. It is known from literature that ^{99m}Tc-pertechnetate accumulates in the thyroid gland [17] and, to a lesser extent, in the salivary glands [18]. However, it is difficult to precisely distinguish these organs based on SPECT/CT data due to their extremely small size in mice. The maximum accumulation in the neck area was observed 3 h post-injection (SUV 23±3).

A significant amount of ^{99m}Tc-pertechnetate accumulated in the pyloric part of the mouse's stomach (Figure 3c), with the accumulation gradually increasing over time. The maximum accumulation was observed at 3 h post-injection (SUV 24±3). The excretion of ^{99m}Tc-pertechnetate by

 doi:10.20944/preprints202408.0697.v1

the gastric mucosa aligns with previously published data [19]. At 3 h post-injection, radioactivity accumulation was found in parts of the colon containing feces (SUV up to 3.3±0.5).

Immediately after injection, there was a moderate accumulation of ^{99m}Tc-pertechnetate observed in the lungs (SUV up to 1.3±0.2), liver (SUV up to 1.6±0.3), and kidneys (SUV up to 1.4±0.3) (Figure 3c, d). After 24 h, lung activity returned to background levels, while activity in the liver and kidneys remained slightly elevated (SUV 0.16±0.05).

An intense accumulation of radioactivity was detected in the bladder, which increased over time and peaked at 3 h post-injection (SUV 10±2), indicating the excretion of ^{99m}Tc via the renal route. There were no signs of ^{99m}Tc accumulation in muscle tissue or the brain.

2.4. Tumour Uptake of ^{99m}Tc-E1b

The experiment used several transplantable tumour models that were fast-growing, easy to cultivate both in vivo and in vitro, well-characterized, and commonly used in experimental oncology. All of these selected tumour lines showed a high potential for spreading to other parts of the body and were likely to create an altered blood vessel network around the tumour. Additionally, previous studies have shown that the cell lines LL/2 (LLC1) [20], Ca755 [15], EMT6 [21], and 4T1 [22] have a tendency to accumulate specific ligands related to αVβ3-integrin and nucleolin when tested in vivo after grafting. For all of the models studied, a gradual accumulation of ^{99m}Tc-E1b over a 24-h period was observed.

Examples of SPECT/CT images of mice with all types of tumours 3 h after administration of the ^{99m}Tc complex are presented in Figure 4 (you can also Supplementary file S3_table_The tumor to normal tissue ratio dynamics).

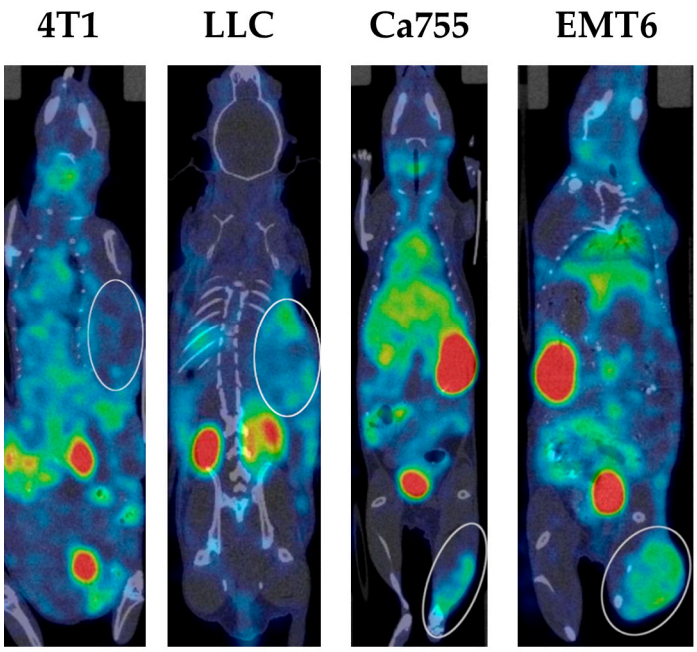

Figure 4. SPECT/CT scan of mice with transplanted tumours at 3 h after ^{99m}Tc-E1b intravenous administration. The tumours 4T1, LLC, Ca755, and EMT6 are indicated by the white ellipse.

The dynamics of the tumour-to-normal tissue ratio (T/N) for ^{99m}Tc-E1b in four syngeneic tumour models are illustrated in Figure 5 and Table 2. At 24 h after administration, the highest T/N ratios were observed for tumours EMT6 (15.7±4.2) and Ca755 (16.5±3.8). Tumours LLC (6.7±4.2) and 4T1 (7.5±3.1) exhibited lower T/N ratios at 24 h after administration.

 doi:10.20944/preprints202408.0697.v1

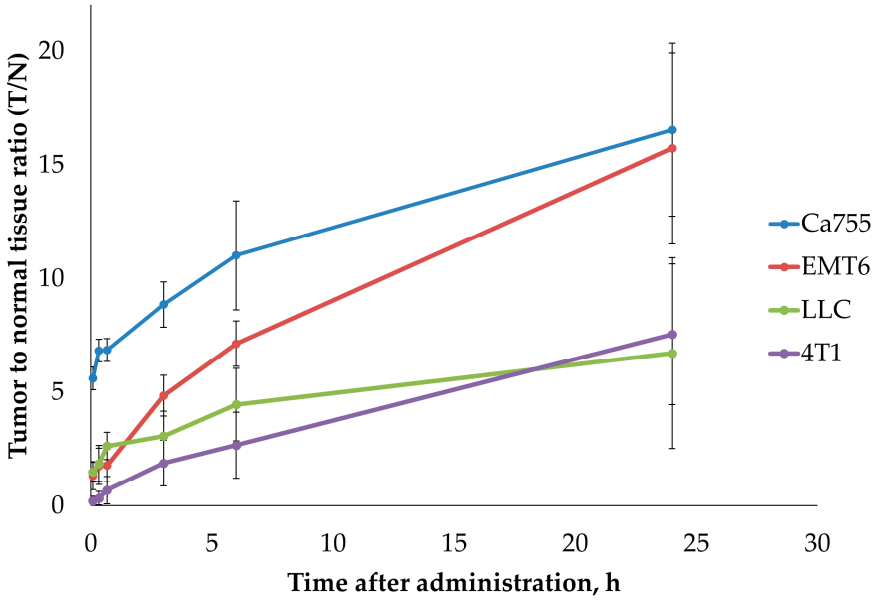

Figure 5. Dynamics of the ratio of the radioactivity in tumour to the radioactivity in muscles as a function of time after administration of ^{99m}Tc-E1b in four transferrable tumour models. The plot specifies the 5, 20, 40 min, 3, 6, and 24 h time points. Each value displayed on the graph is an average SUV value obtained from three animals. The vertical bars represent the standard deviation values.

Table 2. Stoichiometry of functional elements in E1b ^{99m}Tc carrier protein.

T, min	Ca755	EMT6	LLC	4T1
2	5.6±0.5	1.3±0.6	1.5±0.5	0.2±0.2
20	6.8±0.5	1.7±0.8	1.8±0.8	0.3±0.3
40	6.8±0.5	1.8±0.7	2.6±0.6	0.7±0.6
180	8.9±1.1	4.8±0.9	3.1±1.1	1.9±1.0
360	11.0±2.4	7.1±1.0	4.4±1.6	2.7±1.5
1440	16.5±3.8	15.7±4.2	6.7±4.2	7.5±3.1

3. Discussion

The E1b protein used in this study is derived from the previously described E2-13W4 protein [15]. This protein had a completely artificial structure composed of short motifs derived from human proteins, which ensures its immunological compatibility upon administration to the human body. Unlike of most natural proteins, the E1b protein does not have a hydrophobic core. During the design E1b, the sequence encoding GFP was removed from the expression construct of pE2-13W4, and instead, a sequence encoding the C-terminal Cys-rich peptide was added. Such a replacement did not affect the productivity of the *E. coli* strain bearing the corresponding structure: the strains carrying both pE1b and pE2-13W4 showed a protein yield of 18-20 mg/l of the bacterial culture. Noteworthy, both proteins remained completely soluble at the time of synthesis, the inclusion bodies containing the recombinant product were not formed under any cultivation conditions.

Using the recombinant E1b protein as a vehicle for the delivery of ^{99m}Tc to tumours for cancer diagnosis has shown a fairly high efficiency. First of all, the high affinity of the protein for transition metals completely suppressed the accumulation of ^{99m}Tc in the stomach, salivary glands, and thyroid gland, which is characteristic of free ^{99m}Tc administered in the form of sodium ^{99m}Tc-pertechnetate (Table 3).

 doi:10.20944/preprints202408.0697.v1

Table 3. Dynamics of ^{99m}Tc biodistribution administrated to mice in the complex with E1b protein and in the form of sodium ^{99m}Tc-pertechnetate.

Organ	Time point	^{99m}Tc-E1b protein	^{99m}Tc-pertechnetate
heart	5 min	3.5±0.5	2.1±0.3
	20 min	2.1±0.3	1.2±0.2
	40 min	1.4±0.4	0.8±0.2
	2 h	0.6±0.3	
	3 h	0.4±0.2	0.7±0.1
	6 h	0.1±0.1	
	24 h	0.1±0.1	0.05±0.01
lungs	5 min	1.8±0.2	1.3±0.3
	20 min	1.2±0.4	0.9±0.2
	40 min	0.8±0.3	0.6±0.2
	2 h	0.3±0.2	
	3 h	0.2±0.2	0.4±0.1
	6 h	0.07±0.02	
	24 h	0.04±0.02	0.04±0.02
liver	5 min	1.8±0.2	1.6±0.3
	20 min	1.3±0.2	1.5±0.4
	40 min	1.0±0.1	1.4±0.2
	2 h	0.7±0.1	
	3 h	0.6±0.1	0.8±0.2
	6 h	0.5±0.1	
	24 h	0.3±0.1	0.1±0.1
kidneys	5 min	14±1	1.4±0.3
	20 min	18±2	0.9±0.3
	40 min	18±1	0.7±0.2
	2 h	24±6	
	3 h	22±5	0.6±0.1
	6 h	22±7	
	24 h	13±1	0.1±0.1
stomach	5 min	0.5±0.1	5±1
	20 min	0.3±0.1	7±1
	40 min	0.2±0.07	12±2
	2 h	0.1±0.05	
	3 h	0.1±0.05	24±2
	6 h	0.08±0.01	
	24 h	0.05±0.01	1.4±0.3
neck (thyroid and salivary gland area)	5 min	0.2±0.1	5±2
	20 min	0.2±0.1	9±2
	40 min	0.1±0.1	12±1
	2 h	0.1±0.1	
	3 h	0.06±0.04	23±3
	6 h	0.02±0.01	
	24 h	0.02±0.01	0.9±0.2
muscle	5 min	0.3±0.1	0.3±0.1
	20 min	0.2±0.1	0.2±0.2
	40 min	0.17±0.07	0.2±0.1
	2 h	0.07±0.05	
	3 h	0.05±0.05	0.1±0.1
	6 h	0.03±0.01	
	24 h	0.02±0.01	0.01±0.01

The E1b protein-bound ^{99m}Tc is primarily excreted through the kidneys, not through the stomach mucosa and salivary glands, which are the main excretion pathways for the isotope in the pertechnetate form (refer to Table 4). Non-specific tissues show moderate retention of the ^{99m}Tc (in the heart and lungs) or negligible retention (in the brain and skeletal muscles). The liver accumulates

 doi:10.20944/preprints202408.0697.v1

little isotope in both cases, indicating that excretion through the bile is only a secondary factor in its overall pharmacodynamics. The retention of the E1b protein-bound isotope in the heart and lungs is somewhat faster and better than the retention of the pertechnetate-bound isotope. However, in both cases, the absolute SUV values are so small that they do not compromise the generally acknowledged toxicological safety of ^{99m}Tc in SPECT/CT diagnostics [11]. These observations suggest that ^{99m}Tc remains tightly bound to the protein during blood circulation. The revealed biodistribution of ^{99m}Tc administered in the form of a complex with the E1b protein suggests that its use for imaging tumours will be highly effective for any tissues, aside from the tumours of the kidneys and, occasionally, the liver.

Table 4. Data about model cell lines used in the study

Name	ATCC No	Properties	Protocol of maintenance	Immune compatibility with mouse-inbred lines	Peculiarities
LL/2 (LLC1)	CRL-1642™	Transplantable lung Lewis adenocarcinoma occurs as three clones Lab, LLCC3 and LLC1. In our study, the clone LLC1 CRL 1642 was used	[23], [24]	C57Bl/6	A traditional model of metastatic growth for the study of resistance to chemotherapeutic agents
Ca755 or Bagg-Jackson Adenocarcinoma	-	Transplantable mammary gland adenocarcinoma of C57/Bl mice	[25]	C57Bl/6	An acknowledged model of triple-negative human breast cancer with a high metastatic potential
EMT6	CRL-2755™	Metastatic mammary adenocarcinoma	[26], [27], [28]	Balb/c	https://www.modelorg.com/en/Wild-type/62797/post_type/4.html The rapid growth of the tumour node begins from 12-15 days after grafting
4T1	CRL-2539™	Mammary adenocarcinoma	[29]	Balb/c	https://currentprotocols.onlinelibrary.wiley.com/doi/abs/10.1002/0471142735.im2002s39 popular model of the human TNM stage IV

The use of the E1b protein significantly increased the attraction of ^{99m}Tc to experimentally transplanted mouse tumours LLC (lung carcinoma), Ca755, and EMT6 (breast carcinoma). This was shown by a longer retention time in the tumour. Within 24 h after injection, there was a noticeable increase in the concentration difference between the tumour and healthy tissues, as the normal tissues excreted the substance faster compared to the tumours. However, the effectiveness of the E1b protein was lower in the case of 4T1 compared to other tumours. This was unexpected because 4T1 breast carcinoma is the only one in our study known to contain both nucleolin and αVβ3-integrin on the cell surface [21]. Theoretically, the E1b protein should have shown maximum attraction to 4T1 cells, as it can bind to both αVβ3-integrin ligands (RGD peptides) and nucleolin (F3 peptide). However, it's important to note that the characteristics of grafted tumours may change over time, and we lack

 doi:10.20944/preprints202408.0697.v1

experimental data on the abundance of nucleolin and αVβ3-integrin in the 4T1 culture used in the experiment or in other cell lines. Furthermore, reports suggest that specific obstacles in real tumours can hinder the interaction of HER2-positive tumours with HER2-specific antibodies in animal models [5]. Similar mechanisms may also affect the use of ligand-specific isotope carriers in our case and in other cases. Given that most human tumours carry either αVβ3-integrin, nucleolin, or both of these markers on their surface, it is reasonable to assume that a promising radiopharmaceutical based on the E1b protein could be a fairly universal tool for the primary diagnosis of cancer using SPECT/CT. The protein labeling protocol proposed here shows good reproducibility (refer to Supplemental file S4_table_Labeling E1b protein), yields a high level of radioactivity of about 294 MBq per mg E1b protein immediately after the purification step, as well as tight binding of ^{99m}Tc to the protein.

The use of a centrifuge gel filtration column enables the rapid removal of sodium ^{99m}Tc-pertechnetate, sodium borohydride, and their by-products that did not react with the protein in just 2 min. This efficient process is crucial in clinical trials. The significant difference in MW between the protein and salts allows reliable separation using this simple method, making it suitable for routine clinical diagnosis. It is anticipated that this technique will reduce the toxicity of a ^{99m}Tc-based diagnostic radiopharmaceutical, potentially based on the E1b protein. The E1b protein is expected to compete with existing commercial SPECT-compatible carriers for ^{99m}Tc, offering advantages such as fast clearance of most of the isotope after 6 h and a continuously increasing tumour to overall normal tissue ratio for 24 h. These pharmacokinetic properties have not been reported previously for any other ^{99m}Tc carrier, making it favorable for the early detection of small tumour foci, provided that SPECT/CT tomographs have adequate sensitivity.

4. Materials and Methods

4.1. Chemicals and Disposables

$NaBH_4$ (16940-66-2), LB broth (Luria low salt, L3397-250G), lysozyme from chicken egg, AEBSF (A8456-25MG), and other chemicals were obtained from Sigma-Aldrich (St. Louis, MO, USA). HisPur™ Ni-NTA Resin (88221), PD-10 gravity flow desalting column (G 25), Zeba™ Spin Desalting Columns, 7K MWCO (89891) and the Pierce™ BCA Protein Assay Kit (23227) were purchased from Thermo Fisher Scientific (USA). Additionally, a sterile saline solution of 0.15 M NaCl (pH 7.4) was acquired from PanEco (Russia). Sodium ^{99m}Tc-pertechnetate was fresh eluted from ^{99m}Tc generator GT 4K manufactured by L.Y. Karpov NIPCI (Russia).

4.2. Genetic Constructs

The pRSET-EmGFP plasmid (V35320, Thermo Fisher Scientific) was used as a vector for the expression of the ^{99m}Tc-carrier protein. High-fidelity restriction endonucleases (BamHI-HF, XhoI) and T4-DNA-ligase were purchased from New England Biolabs (Ipswich, MA, USA). The oligonucleotides were synthesized using the solid-phase method and purified by preparative polyacrylamide gel electrophoresis (PAGE) by Syntol LLC (Russia). Q5® High-Fidelity DNA Polymerase (New England Biolabs, USA) was used for all preparative polymerase chain reactions (PCR). Ultrafree-DA Centrifugal Filter Units (42600, Merck, NJ, USA) were used for DNA extraction from agarose gel. The ZymoPURE™ Plasmid Miniprep Kit (Zymo Research, Irvine, CA, USA) was used for plasmid DNA purification. The authenticity of the plasmids was confirmed by Sanger sequencing performed by Eurogen CJSC (Russia). *E. coli* strain NiCo21(DE3) (C2529H, New England Biolabs, Ipswich, MA, USA) was used for cloning and expression experiments according to the manufacturer's protocol.

4.3. Software

SnapGene Viewer (GSL Biotech LLC, Chicago, IL, USA, available at snapgene.com) was used to design and manage plasmid maps. Oligo Analyzer 1.0.3, a free software program developed by T. Kuulasmaa, was used to design oligonucleotides. GelAnalyzer 19.1, a free software program developed by I. Lázár, was used for digital gel densitometry. Protein properties were predicted by

 doi:10.20944/preprints202408.0697.v1

using the Protein Calculator v3.4 free online tool (https://protcalc.sourceforge.net/). Image reconstruction (SPECT and CT) was performed using the built-in MiLabs Rec 12.00 software. The processing of SPECT/CT images was carried out using PMOD 4.205 software (PMOD Technologies LLC, Switzerland).

4.4. Murine Tumour Cell Cultures

Cell lines Lewis lung adenocarcinoma (ATCC CRL-1642), mammary adenocarcinoma Ca755 (or Bagg-Jackson adenocarcinoma), metastatic mammary adenocarcinoma EMT6 (ATCC CRL-2755™), mammary adenocarcinoma 4T1 (ATCC CRL-2539™) were obtained from the Blokhin National Medical Research Center of Oncology of the Ministry of Health of the Russian Federation (Blokhin NMRCO) cell collection. Details about the model cell lines utilized in the study can be found in Table 4.

4.5. Production and Purification of E1b Protein

4.5.1. Genetic Construct pE1b

The plasmid pE2-13W4, previously described [15], was used as the source. Initially, a 4,067 bp long PCR product was obtained using the pE2-13W4 plasmid as a template and a pair of primers: GFPmin-for cgaccacatgaagcagcacgac and GFPminBam-rev ccatggtggcgaaggatccgctaccagg. Thus, the BamHI restriction site was introduced at the end of the coding region. After purification, the PCR product was cleaved with BamHI HF and XhoI restriction enzymes following the manufacturer's protocol. A 3,558 bp long BamHI/XhoI PCR product was purified from an agarose gel after preparative electrophoresis.

An insert encoding a 12 amino acid Cys-containing flexible peptide (GGGCGGGCGGGC) with subsequent stop codon was assembled from a pair of complementary oligonucleotides: C3-for gatccggtggcggttgcggtggcggttgtggtgttgttaac and C3-rev tcgagttaacaaccgccaccacaaccgccaccgcaaccgccaccg (Syntol, Russia), generating sticky ends for restriction sites BamHI and XhoI upon duplex formation. It was then ligated with the pre-prepared vector described in the previous paragraph. The *E. coli* strain NiCo21(DE3), recommended for efficient expression, was immediately transformed with a DNA mix after ligation. The sequence of the E1b protein gene in the expression construct was confirmed by restriction mapping, PCR with specific primers, and Sanger sequencing (Eurogen, Russia).

4.5.2. E1b Protein Production and Purification

The recombinant *E. coli* strain derived from NiCo21 (DE3, pE1b) was cultured in a complete LB medium (composed of 10 g/l peptone, 5 g/l yeast extract, and 10 g/l NaCl), supplemented with 100 mg/l ampicillin, for 24 h at 37°C. The harvested cells were lysed and used to purify the recombinant protein, following the previously described method [15]. The purification process involved metal chelate chromatography (IMAC) using HisPur™ Ni NTA resin and the removal of metal ions from metal-binding sites through extensive dialysis after EDTA treatment. The purity of the E1b protein preparation was confirmed using denaturing disc electrophoresis in a polyacrylamide gel with sodium dodecyl sulfate (SDS-PAGE). The protein concentration was determined using a modified Lowry method with a bicinchoninic acid (BCA) assay kit from Sigma, following the manufacturer's recommendations. The presence of free sulfhydryl groups in the protein preparation was evaluated by reacting with DTNB as described previously [30].

4.6. Labeling E1b protein with ^{99m}Tc and purification of the complex

The experiment was conducted in a specially designed enclosure with a protective screen to adhere to safety regulations for handling radioactive materials. Along the study, the ^{99m}Tc labeling procedure was repeated several times, and the resulting preparation could vary slightly in radioactivity (refer to Supplementary file S4_table_Labeling E1b protein). We standardized the

 doi:10.20944/preprints202408.0697.v1

administered dose (~80 MBq for each mouse) by slightly varying the injection volume of the preparation. The typical labeling protocol is described below. Initially, 280 µL of a ^{99m}Tc solution (~995.4 MBq), 0.018 g (0.476 mmol) of $NaBH_4$, and 700 µL (2.3 mg) of protein E1b were mixed to achieve a final volume of 1 ml. The mixture was then left to incubate for 30 min at room temperature (18-20°C) before being desalted using Zeba™ Spin Desalting Columns with a 7K MWCO, as per the manufacturer's instructions, using sterile saline at pH 7.2. The radioactivity of the eluate was immediately measured and approximately 80 MBq (about 120 µl) of the eluate was injected intravenously into a mouse. A control group of mice was administered an equivalent radioactivity of free sodium ^{99m}Tc-pertechnetate.

4.7. Tumour animal model

All the animal studies were conducted in compliance with local ethical regulations and were approved by the institutional ethics committee (Protocol No. 2 dated 10.06.2020). The animals were maintained in accordance with the rules of the European Convention for the Protection of Vertebrates Used for Research and Other Scientific Purposes [31]. For all in vivo studies, female laboratory mice of the C57Bl/6 and Balb/c lines aged 6-8 weeks and weighing 20-22 g (bred by Blokhin NMRCO) were used. To study the biodistribution of recombinant protein and free ^{99m}Tc-pertechnetate as a reference in healthy mice, 2 groups of Balb/c mice (n=6) were used. Additionally, 4 groups of tumour-bearing mice (n=3 in each group) were formed to assess the accumulation of ^{99m}Tc-E1b protein in solid tumours: 1) C57Bl/6 mice with lung adenocarcinoma LLC, 2) C57Bl/6 mice with mammary adenocarcinoma Ca755, 3) Balb/C mice with mammary adenocarcinoma 4T1, 4) Balb/C mice with breast adenocarcinoma EMT6. The inoculation of all tumour strains was carried out as per [32]. Ca755 and EMT6 tumours were grafted into the right hind leg, and LLC and 4T1 into the right side. Totally, 24 mice were used in the experiment.

During scanning, the animals were anesthetized with a 2% isoflurane air mixture. The animals' condition was monitored by assessing respiratory rate using built-in equipment and BioVet software. Post the SPECT/CT studies, the mice were kept in a vivarium with daily body weight measurements and a general veterinary examination, along with monitoring water and feed consumption. Changes in body weight were consistent with tumour growth, and no changes in water and feed consumption and behavior were noted.

4.8. SPECT/CT In Vivo Imaging

The substance's radioactivity was measured using the Isomed 2010 dose calibrator (MED Nuclear Medizintechnik Dresden Gmb, Germany) before it was administered. A small laboratory animal Vector 6 (MiLabs, the Netherlands) PET/SPECT/CT scanner was used to perform the SPECT/CT study, with a HE-UHR-RM collimator. Both ^{99m}Tc-E1b protein and ^{99m}Tc-pertechnetate compounds were injected intravenously into mice. SPECT scanning began 5 min after the ^{99m}Tc administration and continued for 1 h in 12 frames of 5 min each. Time points at 2 h, 3 h, 6 h, and 24 h after administration were scanned in frames of 10 min, 10 min, 15 min, and 30 min, respectively. For ^{99m}Tc-pertechnetate, the first-hour protocol was the same, and then the data at only 3 h and 24 h were acquired. The image reconstruction (SPECT and CT) was done using the built-in MiLabs Rec 12.00 software. For SPECT reconstruction, the following parameters were chosen: energy window 140±10% keV, SROSEM iterative algorithm, voxel size of 0.8 mm, and radioactive decay correction function. CT images were reconstructed using the Radon transform with a voxel size of 0.2 mm. Subsequently, the software MiLabs Rec 12.00 registered pairs of SPECT and CT images and produced merged SPECT/CT images.

4.9. Processing of SPECT/CT Data

The SPECT/CT images were processed using PMOD 4.205 software from PMOD Technologies LLC, based in Switzerland. We outlined volumes of interest using the CT image of the mouse and calculated the average activity within these outlined volumes (measured in MBq/cc). For the

 doi:10.20944/preprints202408.0697.v1

biodistribution study, we focused on the following organs: heart, lungs, liver, kidneys, bladder, bowel, muscle, and brain. Additionally, for the biodistribution of ^{99m}Tc-pertechnetate, we also examined the stomach and thyroid gland. In mice with tumours, we outlined the tumours, heart, and muscle for quantitative study. Total body radioactivity was determined for all animals. We calculated the standardized uptake value (SUV) for all the studied organs and tissues. To provide a statistical estimate of the SUV value for each organ, we evaluated the mean value for all the animals in each group, with a confidence interval of 95% as ± SD (Standard Deviation).

Supplementary Materials: The following supporting information can be downloaded at Preprints.org.

Author Contributions: Conceptualization, N.V.P. and A.B.S.; methodology, N.V.P., A.A.L., V.A.S, K.E.S., Y.A.F., A.V.S.; software, N.V.P., A.A.L., V.A.S, K.E.S., Y.A.F.; validation, N.V.P., A.A.L., V.A.S, K.E.S., Y.A.F., A.V.S.; formal analysis, A.A.L., V.A.S, K.E.S., Y.A.F.; investigation, N.V.P.; resources, E.Y.G., A.A.L. and A.B.S.; data curation, N.V.P., A.A.L., V.A.S, K.E.S., Y.A.F., A.V.S.; writing—original draft preparation, N.V.P. and A.B.S.; writing—review and editing, N.V.P. and A.B.S.; visualization, N.V.P., A.A.L., V.A.S, K.E.S., Y.A.F., A.V.S.; supervision, E.Y.G.; project administration, N.V.P. , A.A.L. and A.B.S.; funding acquisition, E.Y.G. and A.B.S.

Funding: The research was carried out with the financial support of the Additional Agreement to State Assignment No. 075-03-2023-346/1 since February 27, 2023.

Institutional Review Board Statement: The study was conducted in accordance with the Declaration of Helsinki, and approved by the Institutional Review Board (or Ethics Committee) of N.N. Blokhin NMRCO (Protocol No. 2 dated 10.06.2020). All the animal studies were conducted in compliance with local ethical regulations and were approved by the institutional ethics committee.

Data Availability Statement: The data that support the findings of this study are included in this published article and its Supplementary Information files.

Acknowledgments: The authors appreciate the staff of the Radionuclide Diagnostics Department №1 (Radionuclide Diagnostics and Therapy Section) of Blokhin NMRCO for providing 99mTc.

Conflicts of Interest: The authors declare no conflicts of interest.

Abbreviations

^{99m}Tc	Technetium-99m (^{99m}Tc) is a metastable nuclear isomer of technetium-99 symbolized as ^{99m}Tc
ELP repeats	Elastin-like polypeptides
SPECT	Single-Photon Emission Computed Tomography
CT	X-ray Computed Tomography
G4EC	oligopeptide with amino acid composition GGGGEC
HER-2	cancer marker (epidermal growth factor receptor)
TNFα	tumor necrosis factor α
SUV	standardized uptake value
His-tags	a polyhistidine-tag is an amino acid motif in proteins that typically consists of at least six histidine (His)
T/N ratio	tumor-to-normal tissue ratio
SCID	severe combined immunodeficiency
RGD	peptide - peptide containing the RGD (Arginylglycylaspartic acid)
F3 peptide	A 31 amino acid fragment of HMGN2 protein, specifically bound to the nucleolin oncomarker
GFP	green fluorescent protein
E. coli	Escherichia coli

 doi:10.20944/preprints202408.0697.v1

IMAC	Immobilized Metal Chelate Affinity Chromatography
^{99m}Tc-E1b	tight complex of ^{99m}Tc radioactive isotopes and E1b protein
EDTA	ethylenediaminetetraacetic acid
SDS-PAGE	sodium dodecyl sulfate (SDS) polyacrylamide gel electrophoresis
PAAG	polyacrylamide gel
DTNB	Ellman's reagent, 5,5′-dithiobis-(2-nitrobenzoic acid)
E2-13W4	protein composed from multiple metal-binding centers and the universal tumor-specific ligands:RGD (Arg-Gly-Asp) and F3-peptide (nucleolin-binding peptide)
BCA	bicinchoninic acid
ATCC	American Type Culture Collection
Blokhin NMRCO	Blokhin National Medical Research Center of Oncology of the Ministry of Health of the Russian Federation
MW	molecular weight

Appendix A. The Procedure for Contouring Organs up on SPECT/CT

The following organs and tissues were selected to determine SUV: heart, lungs, neck (thyroid and salivary glands), liver, spleen, intestines, muscle tissue, stomach, kidneys. SPECT processing/CT scans (fusion, selection of areas of interest and obtaining their parameters, assessment of specific activity) were performed using the PMOD software package (PMOD Technologies LLC, Switzerland).

The organs and tissues were contoured by CT tomography, because SPECT tomograms do not always provide a sufficiently clear definition of the boundaries of tissues and organs due to limited spatial resolution. In turn, CT has a high spatial resolution, which makes it possible to more accurately determine the boundaries of structures and organs.

Contouring of all organs was performed using the Polygon tool. First, the area of interest was selected, and then the first contour was drawn, with orientation to the center of the organ. The following contours were drawn through several sections; the process was repeated several times. Using the Contour Interpolation tool, the contours were combined, which allowed reconstructing a three-dimensional image.

 doi:10.20944/preprints202408.0697.v1

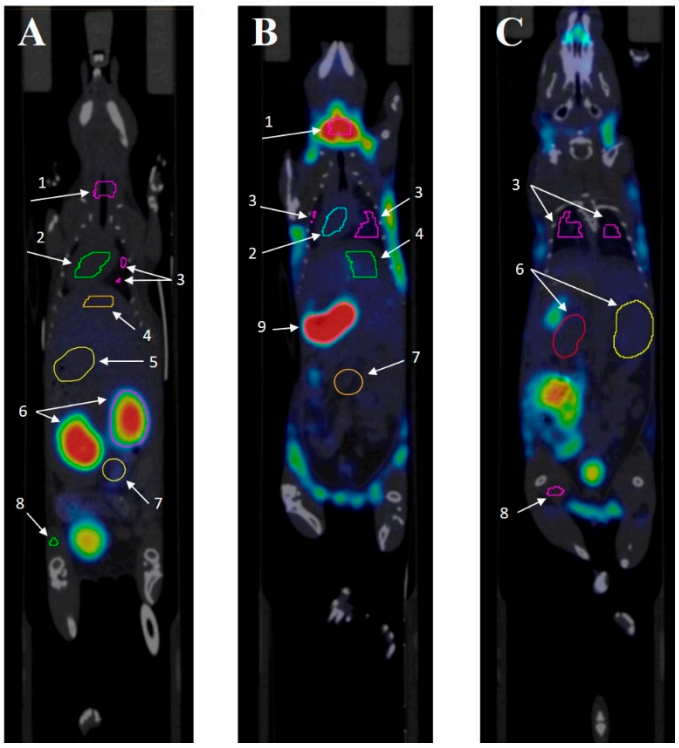

Figure A1. A. PET/CT of intact mouse №1 from ^{99m}Tc-E1b bio distribution group, coronal section at kidney level, 3 hours after administrating the contrast. **B**. PET/CT scan of intact mouse №2 from ^{99m}Tc pertechnetate bio distribution group, coronal section at the level of the stomach and thyroid gland, 3 hours after administrating the contrast. **C**. PET/CT scan of the same intact mouse №2 from the ^{99m}Tc pertechnetate biodistribution group, coronal section at kidney level, 3 hours after administrating the contrast. *Organs:* thyroid gland area (1), heart (2), lungs (3), liver (4), stomach area (5), kidneys (6), intestines (7), muscle tissue (8).

References

1. Li, W.; Zhang, L.; Li, W.; Zhang, R. The Value of ^{99m}Tc-Methylene Diphosphonate Single-Photon Emission Computed Tomography/Computed Tomography in Detecting Atraumatic Costal Cartilage Fracture in Malignant Tumor Patients. *Frontiers in oncology*. **2020**, *10*, 138. DOI: 10.3389/fonc.2020.00138
2. Cole, T.J.; Balseiro, J.; Lippman, H.R. Technetium-99m-methylene diphosphonate (MDP) uptake in a sympathetic effusion: an index of malignancy and a review of the literature. *J Nucl Med.* **1991**, *32*, 325–327.
3. Wu, C.; Yang, S.; Sun, Z.; Han, X.; Ye, Y.; Liu, S. Characterization of the attenuation of breast cancer bone metastasis in mice by zoledronic acid using (99m)Tc bone scintigraphy. *Pathol Oncol Res.* **2014**, *20*, 747–754. DOI: 10.1007/s12253-014-9756-z
4. Ranadive, G.N.; Rosenzweig, H.S.; Epperly, M.W.; Seskey, T.; Bloomer, W.D. A new method of technetium-99m labeling of monoclonal antibodies through sugar residues. A study with TAG-72 specific CC-49 antibody. *Nucl Med Biol.* **1993**, *20*, 719–726. DOI: 10.1016/0969-8051(93)90158-q
5. Li, L.; Liu, T.; Shi, L.; Zhang, X.; Guo, X.; Hu, B.; Yao, M.; Zhu, H.; Yang, Z.; Jia, B.; et al. HER2-targeted dual radiotracer approach with clinical potential for noninvasive imaging of trastuzumab-resistance caused by epitope masking. *Theranostics* **2022**, *12*, 5551–5563. DOI: 10.7150/thno.74154
6. Shi, D.; Fu, W.; Tan, H.; Lin, Q.; Shi, H.; Cheng, D. Preclinical Evaluation of ^{99m}Tc-MAG$_3$-5-Fab Targeting TREM2 in Lung Cancer Mouse Models: A Comparison with ^{99m}Tc-MAG$_3$-5-F(ab')$_2$. *Mol Pharm.* **2024**, *21*, 303–312. DOI: 10.1021/acs.molpharmaceut.3c00870
7. Delvaeye, T.; Wyffels, L.; Deleye, S.; Lemeire, K.; Gonçalves, A.; Decrock, E.; Staelens, S.; Leybaert, L.; Vandenabeele, P.; Krysko, D.V. Noninvasive Whole-Body Imaging of Phosphatidylethanolamine as a Cell Death Marker Using ^{99m}Tc-Duramycin During TNF-Induced SIRS. *J Nucl Med.* **2018**, *59*, 1140–1145. DOI: 10.2967/jnumed.117.205815

8. Stafford, J.H.; Thorpe, P.E. Increased exposure of phosphatidylethanolamine on the surface of tumor vascular endothelium. *Neoplasia* **2011**, *13*, 299–308. DOI: 10.1593/neo.101366
9. Cappenberg, T.M; De Schepper, S.; Vangestel, C.; De Lombaerde, S.; Wyffels, L.; Van den Wyngaert, T.; Mattis, J.; Gray, B.; Pak, K.; Stroobants, S.; et al. First-in-human study of a novel cell death tracer [^{99m}Tc]Tc-Duramycin: safety, biodistribution and radiation dosimetry in healthy volunteers. *EJNMMI Radiopharm Chem*. **2023**, *8*, 20. DOI: 10.1186/s41181-023-00207-1
10. Chapeau, D.; Koustoulidou, S.; Handula, M.; Beekman, S.; de Ridder, C.; Stuurman, D.; de Blois, E.; Buchatskaya, Y.; van der Schilden, K.; de Jong, M.; et al. [^{212}Pb]Pb-eSOMA-01: A Promising Radioligand for Targeted Alpha Therapy of Neuroendocrine Tumors. *Pharmaceuticals (Basel).* **2023**, *16*, 985. DOI: 10.3390/ph16070985
11. Veres, D.S.; Máthé, D.; Hegedűs, N.; Horváth, I.; Kiss, F.J.; Taba, G.; Tóth-Bodrogi, E.; Kovács, T.; Szigeti, K. Radiomic detection of microscopic tumorous lesions in small animal liver SPECT imaging. *EJNMMI Res.* **2019**, *9*, 67. DOI: 10.1186/s13550-019-0532-7
12. Boschi, A.; Uccelli, L.; Martini, P. A Picture of Modern Tc-99m Radiopharmaceuticals: Production, Chemistry, and Applications in Molecular Imaging. *Appl. Sci.* **2019**, *9*, 2526. DOI: 10.3390/app9122526
13. Lanteigne, D.; Hnatowich, D.J. The labeling of DTPA-coupled proteins with 99mTc. *Int J Appl Radiat Isot.* **1984**, *35*, 617–621. DOI: 10.1016/0020-708x(84)90106-6
14. Badar, A.; Williams, J.; de Rosales, R.T.; Tavaré, R.; Kampmeier, F.; Blower, P.J.; Mullen, G.E. Optimising the radiolabelling properties of technetium tricarbonyl and His-tagged proteins. *EJNMMI Res.* **2014**, *4*, 14. DOI: 10.1186/2191-219X-4-14
15. Pozdniakova, N.V.; Ryabaya, O.V.; Semkina, A.S.; Skribitsky, V.A.; Shevelev, A.B. Using ELP Repeats as a Scaffold for De Novo Construction of Gadolinium-Binding Domains within Multifunctional Recombinant Proteins for Targeted Delivery of Gadolinium to Tumour Cells. *Int J Mol Sci.* **2022**, *23*, 3297. DOI: 10.3390/ijms23063297
16. Okada, S.; Vaeteewoottacharn, K.; Kariya, R. Application of Highly Immunocompromised Mice for the Establishment of Patient-Derived Xenograft (PDX) Models. *Cells* **2019**, *8*, 889. DOI: 10.3390/cells8080889
17. Franken, P.R.; Guglielmi, J.; Vanhove, C.; Koulibaly, M.; Defrise, M.; Darcourt, J.; Pourcher, T. Distribution and dynamics of (99m)Tc-pertechnetate uptake in the thyroid and other organs assessed by single-photon emission computed tomography in living mice. *Thyroid.* **2010**, *20*, 519–526. DOI: 10.1089/thy.2009.0213
18. Tanwar, K.S.; Rana, N.; Mittal, B.R.; Bhattacharya, A. Early Quantification of Salivary Gland Function after Radioiodine Therapy. *Indian J Nucl Med.* **2021**, *36*, 25–31. DOI: 10.4103/ijnm.IJNM_158_20
19. Ren, Y.; Jiang, G.; Meng, Y.; Chen, J.; Liu, J. ^{99m}Tc-pertechnetate thyroid static scintigraphy unexpectedly revealed ectopic gastric mucosa of upper esophagus. *Hell J Nucl Med.* **2023**, *26*, 157–159. DOI: 10.1967/s002449912580
20. Niu, S.W.; Wu, C.H.; Chen, H.C.; Yang, C.J.; Chang, J.M.; Chang, E.E.; Chuang, H.H.; Chiu, Y.W.; Zhen, Y.Y.; Hung, C.C.; et al. Proteins Secreted by Lung Cancer Cells Induce the Onset of Proteinuria via Focal Adhesion Kinase Signaling in Mice. *Lab Invest.* **2023**, *103*, 100156. DOI: 10.1016/j.labinv.2023.100156
21. Picchio, M.; Beck, R.; Haubner, R.; Seidl, S.; Machulla, H.J.; Johnson, T.D.; Wester, H.J.; Reischl, G.; Schwaiger, M.; Piert, M. Intratumoral spatial distribution of hypoxia and angiogenesis assessed by 18F-FAZA and 125I-Gluco-RGD autoradiography. *J Nucl Med.* **2008**, *49*, 597–605. DOI: 10.2967/jnumed.107.046870
22. Garone, M.E.; Chase, S.E.; Zhang, C.; Krendel, M. Myosin 1e deficiency affects migration of 4T1 breast cancer cells. *Cytoskeleton (Hoboken)* 2023, *Online ahead of print*. DOI: 10.1002/cm.21819
23. Bertram, J.S.; Janik, P. Establishment of a cloned line of Lewis Lung Carcinoma cells adapted to cell culture. *Cancer Lett.* **1980**, *11*, 63–73. DOI: 10.1016/0304-3835(80)90130-5
24. Sharma, S.; Stolina, M.; Lin, Y.; Gardner, B.; Miller, P.W.; Kronenberg, M.; Dubinett, S.M. T cell-derived IL-10 promotes lung cancer growth by suppressing both T cell and APC function. *J Immunol.* **1999**, *163*, 5020–5028.
25. Straus, M.J.; Sege, V.; Choi, S.C. The effect of surgery and pretreatment or posttreatment adjuvant chemotherapy on primary tumor growth in an animal model. *J Surg Oncol.* **1975**, *7*, 497–512.
26. Rockwell, S.C.; Kallman, R.F.; Fajardo, L.F. Characteristics of a serially transplanted mouse mammary tumor and its tissue-culture-adapted derivative. *J Natl Cancer Inst.* **1972**, *49*, 735–749.
27. Straus, M.J.; Mantel, N.; Goldin, A. The effect of the sequence of administration of cytoxan and methotrexate on the life-span of L1210 leukemic mice. *Cancer Res.* **1972**, *32*, 200–207.

28. Straus, M.J.; Goldin, A. Effects of priming dose schedules in cytoxan treatment of mouse leukemia L1210. *Proc Soc Exp Biol Med.* **1974**, *145*, 1132–1138. DOI: 10.3181/00379727-145-37967
29. Pulaski, B.A.; Clements, V.K.; Pipeling, M.R.; Ostrand-Rosenberg, S. Immunotherapy with vaccines combining MHC class II/CD80+ tumor cells with interleukin-12 reduces established metastatic disease and stimulates immune effectors and monokine induced by interferon gamma. *Cancer Immunol Immunother.* **2000**, *49*, 34–45. DOI: 10.1007/s002620050024
30. Sullivan, M.L.; Bonawitz, N.D. Spectrophotometric determination of reaction rates and kinetic parameters of a BAHD acyltransferase using DTNB (5,5'-dithio-bis-[2-nitrobenzoic acid]). *Plant Sci.* **2018**, *269*, 148–152. DOI: 10.1016/j.plantsci.2018.01.012
31. Directive 2010/63/EU of the European Parliament and of the Council of the European Union of September 22, 2010 on the protection of animals used for scientific purposes. Available online: URL https://eurlex.europa.eu/LexUriServ/LexUriServ.do?uri=OJ:L:2010:276:0033:0079:EN:PDF (accessed on 30 July 2024)
32. Treshchalina, E.M.; Zhukova, O.S.; Gerasimova, G.K.; Andronova N.V.; Garin A.M. Methodological guidelines for the study of antitumour activity of pharmacological substances. In: *Guidelines for the experimental (preclinical) study of new pharmacological substances*. Ed. by Khabriev, R.U. Medicine: Moscow, Russia, 2005; pp. 637–651 (In Russ.).